

A deep learning approach for fault diagnosis of hydrogen fueled micro gas turbines

Muhammad Baqir Hashmi ^{a, *}, Mohammad Mansouri ^{a, b}, Amare Desalegn Fentaye^c, Shazaib Ahsan^d

^a*Department of Energy and Petroleum Engineering, University of Stavanger, 4036, Stavanger, Norway,*

^b*NORCE Norwegian Research Centre, 4021, Stavanger, Norway,*

^c*School of Business, Society and Engineering, Mälardalen University, 883, SE-72123 Västerås, Sweden,*

^d*Department of Mechanical Engineering, University of Manitoba, Winnipeg, Manitoba, R3T 5V6, Canada*

Corresponding author email : muhammad.b.hashmi@uis.no

Abstract

Hydrogen fueled gas turbines are susceptible to rigorous health degradation in form of corrosion and erosion in the turbine section of a retrofitted gas turbine due to drastically different thermophysical properties of flue gas stemming from hydrogen combustion. In this context fault diagnosis of hydrogen fueled gas turbines becomes indispensable. To authors knowledge, there is a scarcity of fault diagnosis studies for retrofitted gas turbines considering hydrogen as a potential fuel. The present study, however, develops an artificial neural network (ANN) based fault diagnosis model using MATLAB environment. Prior to fault detection, isolation and identification modules, physics-based performance data of 100 kW micro gas turbine (MGT) was synthesized using GasTurb tool. ANN based classification algorithm showed a 99.4% classification accuracy of fault detection and isolation. Moreover, the feedforward neural network-based regression algorithm showed quite good training, testing and validation accuracies in terms of root mean square error (RMSE). The study revealed that presence of hydrogen induced corrosion fault (both as single corrosion fault or as simultaneous fouling and corrosion) led to false alarms thereby prompting other wrong faults during fault detection and isolation modules. Additionally, performance of fault identification module for hydrogen fuel scenario was found to be marginally lower than that of natural gas case due to assuming small magnitudes of faults arising from hydrogen induced corrosion.

1. Introduction

The power sector was responsible for ~38% of the global carbon dioxide emissions in 2021. Natural gas (NG) reportedly contributed to ~22% of the electric power generation globally in 2021 (EDGAR/JRC. 2022). By far, gas turbines are mainly burning NG for power generation resulting in greenhouse gas (GHG) emissions and climate change. Therefore, decarbonization of gas turbines becomes indispensable to meet global energy transition mandate. In this context, the gas turbine industry aims for 100% carbon neutral gas fired power generation using low carbon fuels such as hydrogen by 2030 (TURBINE).

Nevertheless, utilization of hydrogen in gas turbines raises several technological and reliability challenges due to radically different thermophysical properties of hydrogen as compared to NG. For instance, hydrogen can potentially lead to flashback and thermoacoustic instabilities in lean premixed dry low emissions / dry low NO_x (DLE/DLN) burners. Flashback can damage the upstream components of the burner. It is worth noticing that

available DLN technologies are currently capable of burning up to 60% hydrogen (Noble et al. 2021). The utilization of 100% hydrogen needs reconfiguration of the gas turbine with a new hydrogen compliant burner and modified fuel system. However, high hydrogen utilization produces enhanced steam content in the combustion flue gas that in turn is responsible for high heat transfer to the metal parts, higher thermal conductivity, aggravated oxidation corrosion, increased creep and thermal fatigue damages of hot gas path components (Gazzani et al. 2014). In this regard, hydrogen fueled gas turbines are susceptible to more health degradation caused by already mentioned problems. Especially, the retrofitted gas turbines, in which solely burner is replaced with hydrogen compliant burner keeping the existing turbomachinery, have more propensity of health degradation. Therefore, intelligent fault diagnosis, prognosis and health monitoring is of crucial importance for enhanced reliability and availability of hydrogen fueled gas turbines. Normally, as the operating hours of gas turbines increase, performance and health degrade due to

various components faults (Marinai, Probert, and Singh 2004). To carry out effective maintenance actions, timely fault detection and identification play a key role in assuring reliability of the engines. Fault diagnosis has been used over the years for industrial and aero gas turbines. It started with Urban's rudimentary concept of linear gas path analysis (GPA) (Urban 1975; Urban and Volponi 1992). Nowadays, gas turbine gas path diagnostic is typically carried out via three methodologies, i.e., model based, data driven and hybrid approaches (Fentaye et al. 2019).

For micro gas turbines, there are a few studies relevant to performance-based fault diagnosis that considered radial compressor fouling, turbine erosion and recuperator degradation phenomena, all considering NG fueled scenarios. Gomes et al., (Gomes et al. 2006) reported that presence of the recuperator in MGT increases the sensitivity of engine to compressor fouling and turbine erosion especially in variable speed operating mode. Hence, they conducted a comparative study of several single and multiple faults i.e., fouling, erosion, foreign object damage (FOD) and recuperator deterioration. The study adopted a model-based approach namely NLGPA technique using Pythia and Turbomatch tools for fault diagnosis. Another study conducted by Yoon et al., (Yoon et al. 2008) employed neural networks for prediction of degraded performance of a 30 kW MGT. Various kinds of single and multiple faults in compressor, turbine and recuperator were included in the study. The approach was found to be predicting the results with much accuracy even if some measurements data were missing.

Talebi and Tousi (Talebi and Tousi 2017) attributed compressor fouling as one of the majorly occurring faults in the MGT engine and hence they investigated the effect of blade surface roughness on the performance degradation of radial turbomachinery in a 477 kW MGT. The study revealed that combustor inlet temperature and turbine outlet temperature were more sensitive to blade surface roughness because these measurements showed increased values than the allowable limits. However, compressor discharge temperature was found to be less sensitive to the roughness. In a similar study, Bauwens (Bauwens 2015) also asserted that compressor fouling was a highly likely occurring fault in a 3 kW MTT MGT because of the possibility of oil ingestion in the compressor originating from de-aerating oil sump. Talebi et al., (Talebi et al. 2022) utilized artificial neural network (ANN) for fault detection and isolation of a 100 kW MGT considering the measurements uncertainties at different part load settings.

After an in-depth literature study, it seems that corrosion study of MGTs fueled by NG is scarce. It was also found that hydrogen induced corrosion in

hot gas path components of both larger gas turbines and MGTs had not been investigated before based on authors' best knowledge. These research gaps paved the way for developing a fault detection, isolation, and identification model for a 100 kW MGT running with pure hydrogen fuel.

The present study incorporates a thermodynamic model using the commercial tool GasTurb 14 for generating a validated design point and off design performance data. Data preprocessing was implicated for adding noise and correcting the data for ambient condition variations. Subsequently, the data was fed to classification and regression learner tools in MATLAB version 2022a for fault detection and diagnosis purposes using neural network approach.

2. Methodology

The overall methodology of the entire study consists of 7-steps as illustrated in Fig. 1.

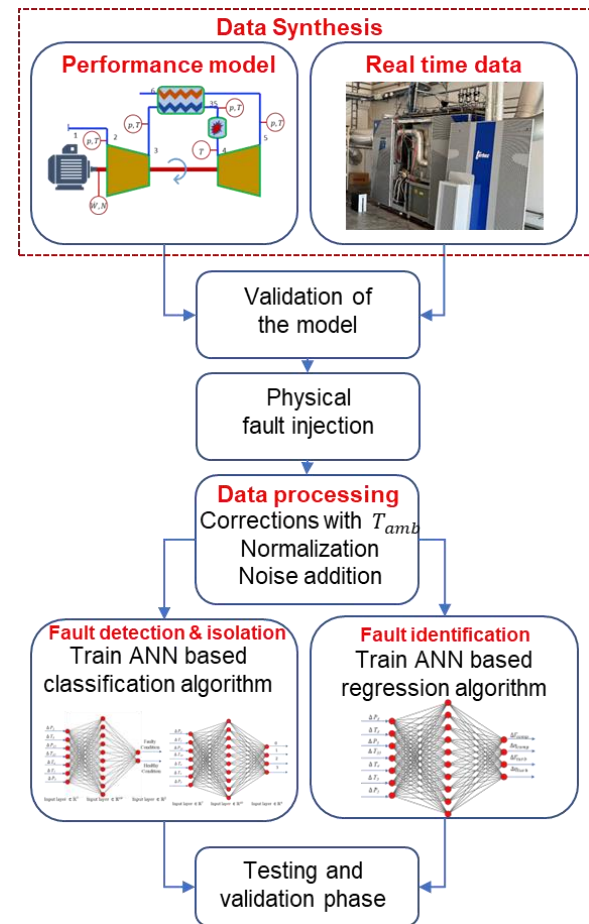


Figure 1: Detailed flow path of the methodology

The process includes developing a physics-based performance model, validating the model with real time MGT data, implanting the physical faults using health parameters i.e., flow capacity and efficiency, processing of synthesized performance data, fault detection and isolation (FDI), fault identification,

and finally testing and validation of the algorithms. Data processing is further segregated into correcting the data against ambient conditions, finding measurement deltas of the signals, and noise addition. Subsequently, the corrected-measured-noisy data of the signals are fed to ANN based classification and regression algorithms for developing a holistic fault diagnosis model. Different steps of the fault diagnosis process are illustrated in Fig. 1. The details of these steps are described in the following sub-sections.

2.1. Baseline performance model

A thermodynamic performance model of a 100 kW MGT was initially developed using commercial software tool GasTurb (Kurzke 2012) for physics-based data generation. The schematic of the MGT with sensor measurement points at various gas path stations is illustrated in Fig. 2.

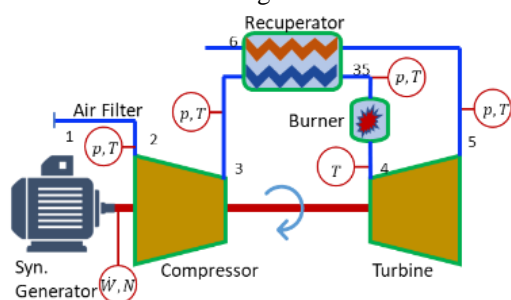


Figure 2. Schematic of a 100 kW MGT

The stations numbers have been identified at their respective positions such as 2 as compressor intake, 3 as compressor exhaust, 35 as recuperator cold side exhaust, 4 as turbine inlet, 5 as turbine exhaust and 6 as recuperator hot side exhaust. The design point calculations were optimized using random search algorithm to assure the accuracy of the baseline model. The off-design performance was calibrated with experimental data for accurate validation purposes. The experiments were conducted at different power settings varying from 50 to 100 kW with a step change of 10 kW. The ambient temperatures were noticed to be varying between 281.15 to 287.15 K during the entire test campaign. The real time data were taken by installing different pressure and temperature sensors in form of probes. To measure gas path conditions at intake of compressor, five pressure and four temperature measuring sensors were installed. Similarly, at compressor exit, three pressure and three temperature measuring sensors were installed 120° apart at circumferential positions to measure the average values at the flow field. Additionally, combustor head was also encompassed with pressure and temperature sensors to measure the conditions of intake air preheated by the recuperator. The instruments used for measuring pressure at different points were Kiel probes installed $\pm 35^\circ$ apart. Pressure scanners were adopted to scan the

pressure with an accuracy of 0.05 of full-scale output. Similarly for temperature measurements K-type thermocouple with an accuracy of ± 1 K were installed, and data acquisition (DAQ) device was utilized to get the measured data. Subsequently, the pressure scanner and DAQ were connected to a computer in parallel mode via two ports which led to data visualization through LabView software. The validated design point data is listed in Tab. 1.

Table 1: Design point validation after optimization

Parameter	OEM data (TURBE C 2017)	Present study	% Error
Power output [kW]	100(± 3)	100.1	0.09
Electrical efficiency [%]	30 (± 1)	29.99	0.03
Pressure ratio [-]	4.5	4.5	0
Exhaust mass flow	0.8	0.799	0.12
Exhaust gas temperature [K]	543	556.83	2.5

The validated off-design data at different part load power settings for different measurement points are illustrated in Fig. 3 and Fig. 4. Firstly, the engine was simulated by assuming NG as a working fuel that basically established a baseline for further model development. Subsequently, hydrogen was utilized as a fuel that was the prime objective of the study. Both simulation scenarios, i.e., NG and hydrogen fuel were further utilized for appending measurement uncertainties along with ambient temperature corrections. Finally, this data was made ready for classification learning and artificial neural network (ANN) to carry out fault detection, isolation, and identification. However, P_3 , T_3 , P_{35} , T_{35} , T_4 , and T_5 , measurement signals were identified as the most significant parameters for fault diagnosis purpose based on their deviating fault signatures.

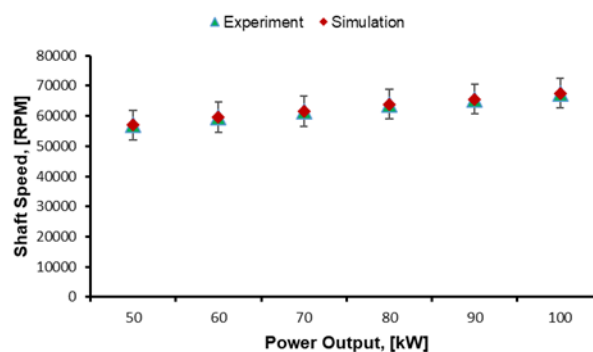


Figure 3. Shaft speed at different power settings

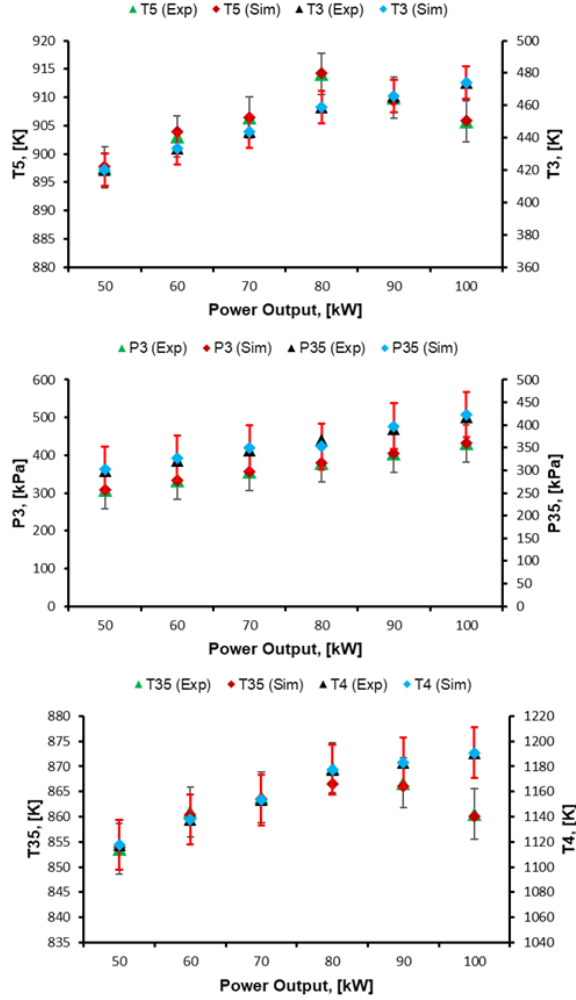


Figure 4: Different pressure and temperatures at various power settings

2.2. Component level degradation

The physical faults such as fouling, corrosion, erosion, and FOD occurring in different components of gas turbine systems lead to variations in engine health parameters or independent parameters i.e., flow capacity and isentropic efficiencies. These health parameters in turn stimulate deviations in engine measurements or dependent parameters such as pressure, temperature, fuel flow and shaft speed. The present study employs the nonlinear GPA (NLGPA) approach for gas path diagnostics of the MGT because of its added advantage over LGPA in terms of accuracy. This is a model-based diagnosis approach that employs a thermodynamic relationship between dependent and independent parameters addressing the nonlinearity of the gas turbine engine. The correlations are as follows,

$$\Delta \vec{Z} = H \cdot \Delta \vec{X} \quad (1)$$

$\Delta \vec{Z}$ is a vector of measurement deviations of a degraded engine condition from clean condition. The clean condition is normally assumed as the healthy condition of the engine at design point. $\Delta \vec{X}$

expresses the health parameters and H represents the influence coefficient matrix (ICM) that develops a correlation between $\Delta \vec{Z}$, and $\Delta \vec{X}$. The further details can be found in the existing literature (Fentaye et al. 2019; Tahan et al. 2017).

The current study encompassed two kinds of component faults i.e., compressor fouling and turbine corrosion. The reason for choosing fouling is due mainly to a higher probability of occurring fouling in recuperated MGT as evidenced by the literature (Gomes et al. 2006; Bauwens 2015). Turbine corrosion was selected because hydrogen fuel leads to an enhanced steam content that can cause higher corrosion and heat transfer rates as compared to a NG fueled gas turbine (Oluyede and Phillips 2007). These hydrogen specific attributes can further lead to aggravated creep and material degradation in hot gas path components and hence to a reduced lifetime of the gas turbine. The quantification of components' physical faults is carried out by developing scaling factors of the health parameters (Flow capacity: Γ , Efficiency: η) as follows,

$$\Gamma_{deg} = \Gamma_{clean} (1 + \Delta\Gamma/100) \quad (2)$$

$$\eta_{deg} = \eta_{clean} (1 + \Delta\eta/100) \quad (3)$$

In the above-mentioned equations, subscript “*deg*” represents degraded component condition while “*clean*” represents engine’s clean or healthy engine condition. Whereas health parameters are represented in their respective symbol as follows, (Flow capacity: Γ , Efficiency: η). However, Δ denotes the change in health parameters. To develop fault diagnosis models for gas turbines, a variety of fault magnitudes have been assumed by the literature that show a relative change of flow capacity and isentropic efficiency from the clean condition in form of scaling or correction factors. Tab. 2 lists the values of compressor and turbine degradation magnitudes with the respective ratios. It is worth mentioning that the fault magnitude of the fouling has been assumed similar for both fuel scenarios while fault magnitude of the hydrogen fuel scenarios has been assumed higher as compared to NG scenarios. The assumption for steam induced corrosion has been borrowed from a study by Zwebek and Pilidis (Zwebek and Pilidis 2004; Zwebek and Pilidis 2003), that was conducted for fault diagnosis of the steam turbine. The reason lies in the fact that steam induced corrosion led by hydrogen fuel behaves similar for both steam turbine and gas turbine.

Table 2: Quantification of various physical faults

Fault	FC (X)	Eff. (Y)	Ratios (X: Y)	Ranges	Ref.
Natural gas case					

CF	$\Gamma_c \downarrow$	$\eta_t \downarrow$	$\sim 3:1$	[0, -7.5] [0, -2.5]	(Qingc ai et al. 2016; Moham madi and Montaz eri-Gh 2014)
TC	$\Gamma_t \uparrow$	$\eta_t \downarrow$	$\sim 2:1$	[0, 4] [0, -2]	(Escher 1995)
Hydrogen case					
CF	$\Gamma_c \downarrow$	$\eta_t \downarrow$	$\sim 3:1$	[0, -7.5] [0, -2.5]	(Qingc ai et al. 2016; Moham madi and Montaz eri-Gh 2014)
TC	$\Gamma_t \uparrow$	$\eta_t \downarrow$	$\sim 2:1$	[0, 5] [0, -2.5]	(Zwebe k and Pilidis 2003; Gomes et al. 2006)

FC: Flow capacity, Eff.: Isentropic efficiency, CF: Compressor fouling, TC: Turbine corrosion

2.3. Fault diagnosis

The diagnosis of the gas turbines is normally performed into three steps i.e., fault detection, fault isolation and finally fault identification. Fault detection provides information about the presence of any imminent physical abnormality in the system. Fault isolation helps in determining the exact type and location of the fault. Fault identification determines the severity magnitude of the any physical fault. The present study incorporated all these steps involved in the diagnosis.

2.3.1. Data processing

Prior to fault diagnosis of the MGT the data generated from the performance model went through preprocessing phase. During preprocessing, the data was first segregated on fuel basis i.e., NG and hydrogen. Subsequently, a fault wise segregation (i.e., compressor fouling, turbine corrosion, and simultaneous compressor fouling and turbine corrosion) was carried out. Temperature corrections was also considered to avoid the influence of the ambient temperature variations on the measurement signals, as follows,

$$\theta = \frac{T_{measured}}{288.15K} \quad (4)$$

The θ , in above equation is the correction factor of the measured temperature ($T_{measured}$) with respect to ambient temperature that is 288.15 K.

Measurement deviations of degraded conditions from clean condition of each signal i.e., P_3 , T_3 , P_{35} , T_{35} , T_4 , T_5 , and P_5 were estimated using the following relation,

$$\Delta \vec{Z} = \frac{(\vec{Z}_{deg} - \vec{Z}_{clean})}{\vec{Z}_{clean}} \times 100 \quad (5)$$

$\Delta \vec{Z}$, in the above equation is the measurement deviation vector between the healthy/clean engine sensors data \vec{Z}_{clean} , and degraded engine's data i.e., \vec{Z}_{deg} . Furthermore, noise was added to the measurement deltas to account for measurement uncertainties that happen in the experimental data. The standard deviation for Gaussian distribution was assumed to be 1% for temperature signals, while 0.5% for pressure signals. The equation involved in the noise generation using random function is as follows,

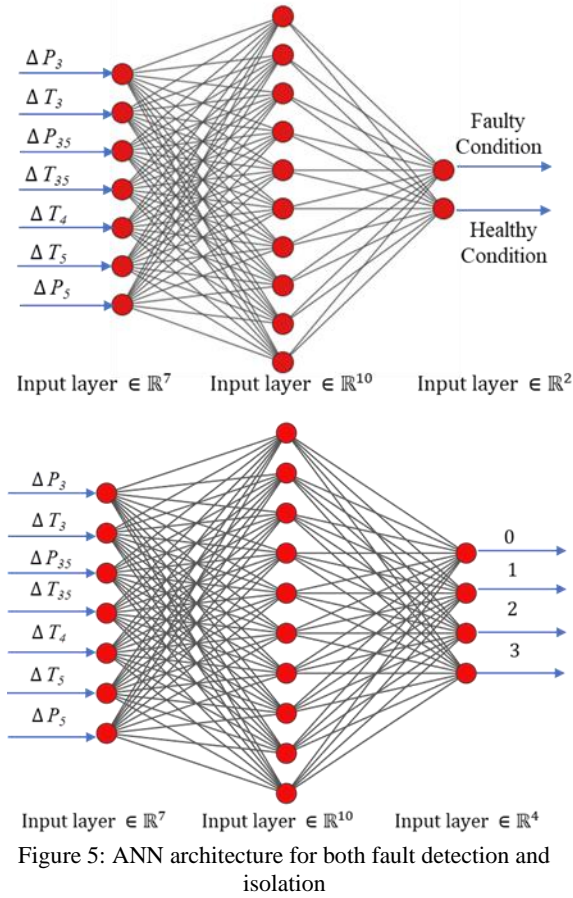
$$x = -1 + 2 \times rand(1, N) \quad (6)$$

N expresses the number of sample points including clean and faulty engine data. A total of 800 sample points were generated, i.e., 400 samples for each NG and hydrogen fuel scenario.

2.3.2. ANN based classification

After accomplishing preprocessing of the data, data were fed to the ANN based classification learner in form of two separate data sets i.e., NG and hydrogen, using MATLAB tool. Using scenarios involved in the labeled data, a classification algorithm "learns" about classifying fresh observations through a supervised machine learning approach. Although, there are plenty of other algorithms for classification learning, the ANN was chosen in the present study. The ANN architecture is show in Fig. 5. The reason for choosing ANN lies in the inherent ability of this algorithm to (i) capture nonlinear behavior of engine performance efficiently (Fentaye et al. 2019), (ii) extract information in fast and simplistic way (Tahan et al. 2017), (iii) handle multiple and larger component faults in presence of sensors faults (Ogaji and Singh 2003), (iv) deal with measurement uncertainties (Marinai, Probert, and Singh 2004), and (v) perform diagnosis with scarcity in measurements (Singh 2003). In classification learner, a validation method needs to be chosen to assess the prediction accuracy of the fitted model. The validation not only provides performance estimations of the model on completely new dataset (as compared to the training dataset), but also helps in protecting against overfitting. The validation scheme chosen in the present study, however, is k -folds cross validation. This scheme works by dissecting the training datasets into k disjoint sets or partitions and then randomly shuffles them. For each round of training-validation, a certain partition is used for validation while the rest of the data is used for testing. Therefore, each partition is used once for validation while $k - 1$, times for training. The k was assumed 5 in the present case based on the data

samples. Cross validation helps in avoiding the overfitting of the training data so that the prediction accuracy might not be compromised.



The classification algorithms finally provide a confusion matrix that determines the number of faults accurately predicted or wrongly predicted. Confusion matrix provides information about the performance of the selected classifier in each class i.e., *True Class* or *Predicted Class*. The rows in the matrix show *True Class*, while the columns represent *Predicted Class*. The diagonal cells depict the matching of both True and Predicted classes. The blue color in the diagonal cells illustrates that the classifier has classified the observations correctly. The confusion matrix plot is also accompanied with two more separated columns on the far-right hand side that show the performance of the classifier per class in terms of *True Positive Rate (TPR)* and *False Negative Rates (FNR)*. *TPR* is basically the proportion of correctly classified observations per true class while *FNR* shows the proportion of the incorrectly classified observation per true class. Another way of determining the classifier performance is by observing the results per *Predicted Class* (instead of *True Class*) in terms of *Positive Predictive Values (PPV)* and *False Discovery Rates (FDR)*. The *PPV* represents the proportion of correctly classified observations per

predicted class. The *FDR* measures how many observations are classified wrongly for each predicted class. The confusion matrix now has summary rows far below the table when this choice was made. *PPV* for properly predicted points in each class are displayed in blue, and *FDR* for erroneously predicted points in each class are displayed in orange.

2.3.3 ANN based fault identification

The final step involved in an MGT diagnosis process is fault identification. The present study utilizes a multi-layer perceptron (MLP) for the intended component fault identification. MLP is a kind of feed forward neural network that works on the concept of supervised learning comprising of input layer, output layer, and one or more hidden layers. In the training phase of the ANN, the network manages to learn the correlations between the input and output data using back propagation algorithm. The current study utilizes a single layer MLP with 10 nodes as shown in Fig. 6. In general, the fault identification is carried out by tracing the health parameters i.e., (Flow capacity: Γ , Efficiency: η) back from the deviated fault signatures. In Fig. 6, on the left-hand side of the ANN structure inputs are provided that have been derived from the equation 5 while the outputs illustrated on right hand side of the structure have been derived from equation 2 and 3. The terms with Δ in the figure represent measurement deviations while Γ and η represents the flow capacity and efficiency of compressor and turbines. The network was trained on the three fault scenarios (CF, TC, CF+TC) to identify some suitable relationships from the fed samples thereby fine tuning the weights and biases. The performance of the training or prediction accuracy is determined by mean square error (MSE) by combining the results from both training and validation data sets. The training progress data and model summary of ANN algorithm have been listed in Tab. 3.

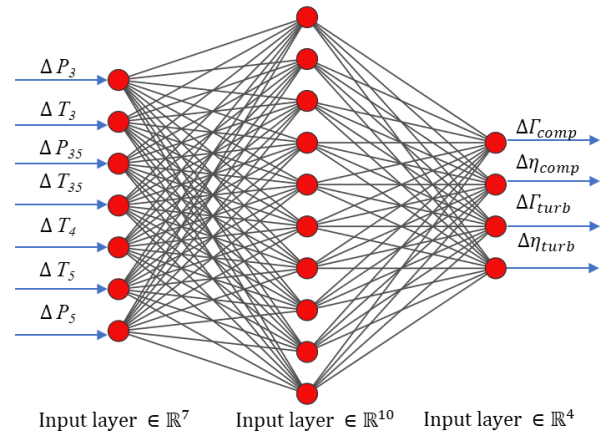


Table 3: ANN training progress data and model summary

Criteria	Indicators
Total hidden layers	1
Neurons in hidden layers	10
Feeding approach	Backpropagation
Target limit of epochs	1000
Performance accuracy target	0
Performance gradient target	1.00e-07
Activation function	Sigmoid
Training algorithm	Levenberg-Marquardt
Performance indicator	Mean square error

3. Results and Discussion

3.1. Fault detection and isolation

For fault detection and isolation, ANN based classifier was employed. Two kinds of data sets were trained, and three fault scenarios were accounted for. For each data set, 70% of the data were utilized for training while the remaining 30% were employed for testing and validation (15% for each) of the algorithm. The performance of the classification algorithm is normally assessed by detection decision matrix and classification confusion matrix consisting of the main decision metrics parameters i.e., True Positive (TP), False Negative (FN), False Positive (FP), and True Negative (TN) as illustrated in Fig. 7. The main diagonal depicts correctly predicted faults while off diagonal show wrongly predicted elements. The detection rates of these decision parameters can be estimated through normalization that is done via dividing each matrix' element by sum of its row's elements as follows (Simon 2010),

$$TPR = \frac{TP}{TP + FN} \times 100\% \quad (7)$$

$$FPR = \frac{FP}{FP + TN} \times 100\% \quad (8)$$

$$FNR = \frac{FN}{TP + FN} \times 100\% \quad (9)$$

$$TNR = \frac{TN}{FP + TN} \times 100\% \quad (10)$$

		Predicted class	
		Fault	No Fault
True Class	Fault	True Positive Detection	False Negative Detection
	No Fault	False Positive Detection	True Negative Detection

Figure 7: Fault detection decision matrix

The selected classification algorithm enables the classification of multiple faults, as shown in Fig. 8. The figure represents the confusion matrix of NG fueled scenario. The labels mentioned on x- and the y-axis represent different fault and no-fault conditions for predicted and true classes respectively, as listed in Tab. 4.

Table 4: Labels of different physical conditions in the classification algorithm

Label	Designated physical condition
0	No fault
1	CF: Compressor fouling
2	TC: Turbine corrosion
3	CF+TC: Simultaneous

It became evident from Fig. 8 that, at no fault condition, the classifier predicted 99.1% correctly as clean, while 0.9 % wrongly predicted as corrosion. Similarly, in row two, 98.2% data points were truly classified as faulty with compressor fouling, while 1.8% was wrongly predicted as non-faulty. The third row depicts that 98.2% samples were correctly predicted as corroded, while 0.9% wrongly predicted as non-faulty and other 0.9% appeared to be wrongly predicting as simultaneous compressor fouling and turbine corrosion. The fourth row, however, shows that 95.5% of the data points were predicted as representing simultaneous fault (CF+TC), while 1.8% wrongly predicted as fouled, and 2.7% wrongly predicted corrosion. The overall positive prediction value (PPV) as shown in Fig. 8 were found as follows, clean condition: 97.3%, fouled: 98.2%, corroded: 96.4%, and simultaneous fouled and corroded: 99.1%. However, the rest of the data samples showed a false detection rate (FDR).

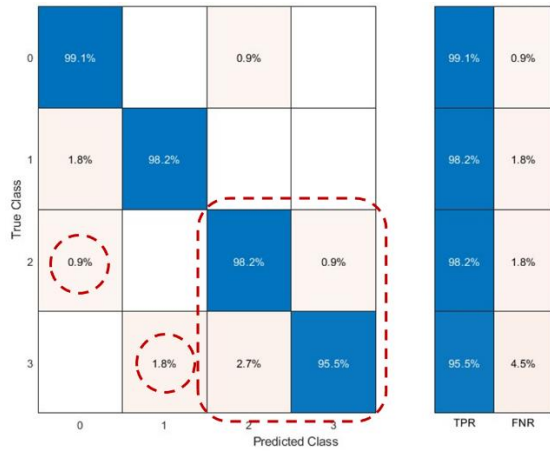


Figure 8: Classification confusion matrix per true class for NG scenario

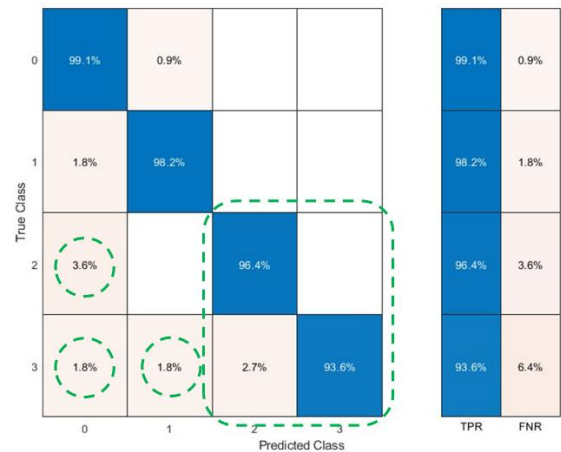


Figure 10: Classification confusion matrix per true class for hydrogen scenario

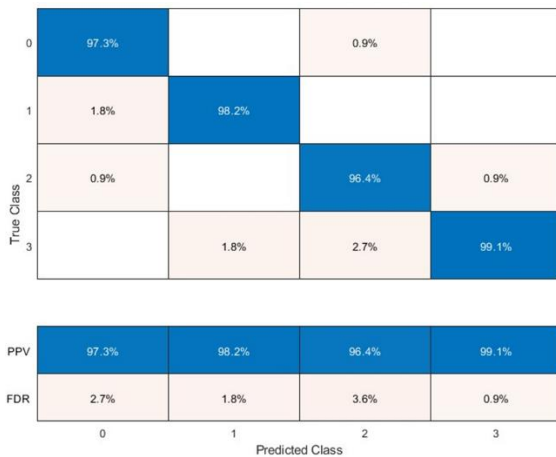


Figure 9: Classification confusion matrix per predicted class for NG scenario



Figure 11: Classification confusion matrix per predicted class for hydrogen scenario

The fault detection and isolation of hydrogen fuel scenario was conducted similarly as NG scenario. The classification confusion matrix of the hydrogen fuel scenario has been illustrated in Fig.10. At clean condition 0.9% wrong prediction of fouling has been indicated, while 99.1% of the data samples were correctly classified as no fault samples. At fouling condition (depicted in row two), 1.8% samples showed a wrong classification as non-faulty, whereas 98.2% were correctly classified as fouled samples. In the corrosion fault, 3.6% data samples were wrongly classified as non-faulty, while 96.4% showed a correct prediction of corrosion fault. Likewise, at simultaneous CF+TC fault, 93.6% data points indicated the simultaneous fault as correctly, while there was wrong prediction of 1.8% as non-faulty, 1.8% as fouled, and 2.7% as corroded components faults.

A comparison of Fig. 8 and 10 for corrosion fault shows that the percentage of wrongly classified faults in hydrogen fuel scenario (3.6%) is more than that of natural gas scenario (1.8%). Similarly, for a simultaneous fault, the utilization of hydrogen fuel is stimulating more wrongly classified fault scenarios i.e., one extra wrongly classified prediction of non-faulty case of 1.8%. The three blue and green dotted circles have been drawn on confusion matrix of both NG and hydrogen scenarios respectively. The green circles are showing extra anomalies in the data as compared to NG one. Among the two anomalies i.e., at cell (2,0), and (3,0) are representing deviation in two of the True classes i.e., corrosion and simultaneous CF+TC. In case of TC, the True class is showing 3.6% wrongly identified faults as non-faulty that is almost double than the NG scenario. Similarly, the simultaneous CF+TC case, is also indicating 1.8% data as wrongly identified as non-faults in presence of the simultaneous CF+T fault. In contrast, in case of NG this wrong non faulty prediction was not observed. However, it is important to mention that the correctly predicted fault rates percentages of a

hydrogen fuel scenario are marginally lower than those of a NG scenario. Additionally, the comparison of Fig. 9 and 11 indicates that PPV of the hydrogen fuel scenario is 100%, while for NG scenario it was 99.1%. It implies that the hydrogen fuel scenario has more propensity of providing positive prediction of faults.

During fault detection, the presence of hydrogen-based corrosion fault led to increased level of incorrectly classified ‘no fault’ as hydrogen induced corrosion fault. Moreover, the simultaneous compressor fouling, and turbine corrosion faults prompted an extra non faulty prediction in contrast with the NG case. It means presence of the hydrogen induced corrosion fault might influence the fault detection process by giving wrong alarm of fault while there is no actual fault.

3.2 Fault identification

The fault identification of the MGT was carried out by using feed forward neural network. The computational framework of the MLP based ANN is through regression analysis. The regression plots of training, testing and validation have been illustrated in Fig. 12. The figure indicates that ANN was able to identify the physical faults parameters with quite good accuracy since the regression values are almost closer to 1. The performance of the ANN prediction is normally evaluated by level of error minimization with respect to the number of epochs (cycles). An epoch is basically the training process of ANN with all the available data at once for one cycle. It is always desirable to keep accuracy as high as possible during the training.

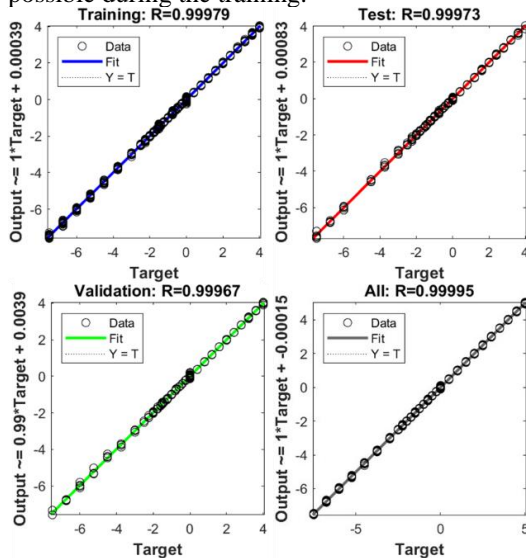


Figure 12: Regression plots for training, testing and validation of a NG fuel ANN model

Normally, a learning curve graph helps in visualizing the convergence of the training, testing and validation; and hence provides information about the accuracy in given epochs. The learning

curve graph keeps on getting better until the model coverages with a minimized error, as shown in Fig. 13.

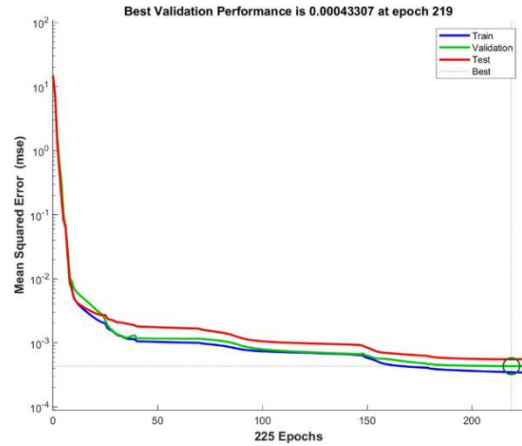


Figure 13: Performance of the ANN training for the NG fuel scenario

The regression of both NG and hydrogen fuel scenarios was found to be nearly identical with similar accuracy as can be observed from Fig. 14. The learning curve-based performance of hydrogen fuel scenario is shown in Fig. 15. The error minimization of the hydrogen scenario took 404 epochs that was significantly greater than that of the NG scenario i.e., 202 epochs.

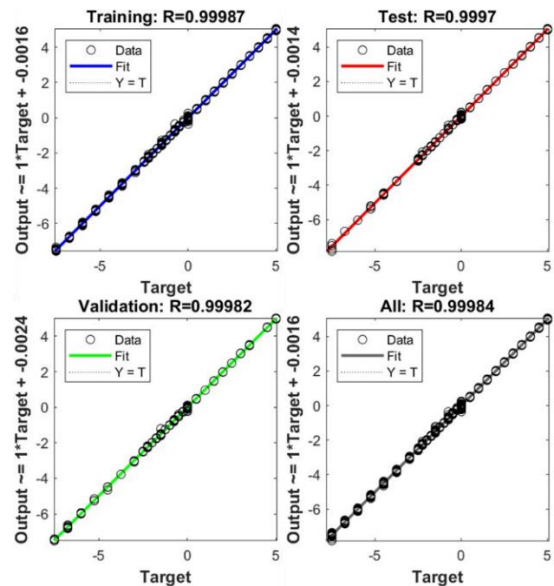


Figure 14: Regression plots for training, testing, and validation of a hydrogen fuel ANN model

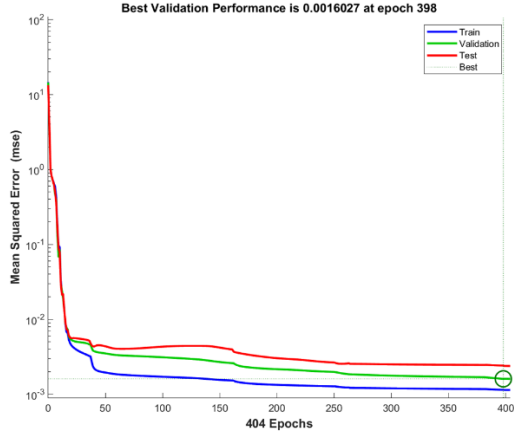


Figure 15: Performance of ANN training for the hydrogen fuel scenario

The overall accuracy of the ANN training, testing and validation was determined by root mean square error (RMSE) using Equation 11. The n , involved in the equation expresses the total sample size, while p_f , and t_f represent the predicted and target fault values. The final results of both MSE and RMSE between the predicted and target values for both NG and hydrogen scenario are listed in Tab. 5. It became evident from the RMSE of the training, testing and validation phases of hydrogen were slightly higher than that of NG scenario.

$$RMSE = \sqrt{MSE} = \sqrt{\frac{1}{n} \sum_{i=1}^n (p_f - t_f)^2} \quad (11)$$

Table 5: Analysis of the fault identification results in terms of RMSE

	MSE NG	MSE Hydroge n	RMSE NG	RMSE Hydroge n
Training	5.92e-4	0.0018	0.0243	0.0424
Testing	6.41e-4	0.0022	0.0253	0.04694
Validation	7.40e-4	0.0032	0.0271	0.0565

4. Conclusion

The study was aimed at developing a fault diagnosis model for a hydrogen fueled MGT in comparison with a NG fueled case. The study involved development of a physics-based model for data generation as an initial step. The data further went through preprocessing phase prior to the fault detection, isolation, and identification. Fault detection and isolation were carried out using an ANN based classification learner, while fault identification was performed using an MLP feed forward ANN. The detection and isolation module showed greater percentages of wrongly classified faults due to involvement of steam induced corrosion in hydrogen fueled scenario as compared

to a NG fired MGT. The hydrogen scenario showed more propensity of positive prediction values too. The performance of fault identification was however, found to be similar for both NG and hydrogen-based scenarios. Further work is needed with increased level of fault severity rising due to steam induced corrosion for better fault identification in hydrogen fueled scenario. The study was part of an initial attempt towards fault diagnosis of hydrogen fueled micro gas turbines. However, further advancements might help the design and maintenance engineers in assuring optimum reliability and availability of the MGT.

Acknowledgments

The authors would like to thank the University of Stavanger, and the Equinor's Akademia program for providing the invaluable support in conducting this research. Mohammad Mansouri would like to acknowledge the Robinson project that has received funding from the European Union's Horizon 2020 research and innovation programme under grant agreement No 957752. It should be noted that this paper reflects only the authors' views, and the Research Executive Agency, Equinor, and the European Commission are not liable for any use that may be made of the information contained therein.

References

- Bauwens, PL. 2015. 'Gas path analysis for the MTT micro turbine'.
- Chen, Yu-Zhi, Xu-Dong Zhao, Heng-Chao Xiang, and Elias Tsoutsanis. 2021. 'A sequential model-based approach for gas turbine performance diagnostics', *Energy*, 220: 119657.
- EDGAR/JRC. 2022. "Global carbon dioxide emissions from 1970 to 2021, by sector (in billion metric tons of carbon dioxide)." In.: Statista.
- Fentaye, Amare D, Aklilu T Baheta, Syed I Gilani, and Konstantinos G Kyprianidis. 2019. 'A review on gas turbine gas-path diagnostics: State-of-the-art methods, challenges and opportunities', *Aerospace*, 6: 83.
- Gazzani, Matteo, Paolo Chiesa, Emanuele Martelli, Stefano Sigali, and Iarno Brunetti. 2014. 'Using hydrogen as gas turbine fuel: premixed versus diffusive flame combustors', *Journal of Engineering for Gas Turbines and Power*, 136.
- Gomes, EEB, D McCaffrey, MJM Garces, AL Polizakis, and P Pilidis. 2006. "Comparative analysis of microturbines performance deterioration and diagnostics." In *Turbo Expo: Power for Land, Sea, and Air*, 269-76.
- Kim, Sangjo, Ju Hyun Im, Myungho Kim, Junghoe Kim, and You Il Kim. 2023. 'Diagnostics using a physics-based engine model in aero gas turbine engine verification tests', *Aerospace Science and Technology*: 108102.
- Kurzke, J. 2012. "GasTurb 12: A program to calculate design and off-design performance of gas turbines. User's manual." In.: GasTurb, Aachen, Germany.
- Marinai, Luca, Douglas Probert, and Riti Singh. 2004. 'Prospects for aero gas-turbine diagnostics: a review', *Applied energy*, 79: 109-26.
- Noble, David, David Wu, Benjamin Emerson, Scott Sheppard, Tim Lieuwen, and Leonard Angello. 2021. 'Assessment of current capabilities and near-term

- availability of hydrogen-fired gas turbines considering a low-carbon future', *Journal of Engineering for Gas Turbines and Power*, 143.
- Oluyede, Emmanuel O, and Jeffrey N Phillips. 2007. "Fundamental impact of firing syngas in gas turbines." In *Turbo expo: power for land, sea, and air*, 175-82.
- Tahan, Mohammadreza, Elias Tsoutsanis, Masdi Muhammad, and ZA Abdul Karim. 2017. 'Performance-based health monitoring, diagnostics and prognostics for condition-based maintenance of gas turbines: A review', *Applied energy*, 198: 122-44.
- Talebi, SS, A Madadi, AM Tousi, and M Kiaee. 2022. 'Micro Gas Turbine fault detection and isolation with a combination of Artificial Neural Network and off-design performance analysis', *Engineering Applications of Artificial Intelligence*, 113: 104900.
- Talebi, SS, and AM Tousi. 2017. 'The effects of compressor blade roughness on the steady state performance of micro-turbines', *Applied Thermal Engineering*, 115: 517-27.
- TURBEC, SPA. 2017. "Technical Description Microturbine Turbec T100. people. unica. it/danielecocco/files/2012/07/Microturbina_T100_Detailed_Specifications1. pdf." In.: Stand.
- TURBINE, ZERO-CARBON GAS. 'HYDROGEN GAS TURBINES'.
- Urban, Louis A. 1975. 'Parameter selection for multiple fault diagnostics of gas turbine engines'.
- Urban, Louis A, and Allan J Volponi. 1992. 'Mathematical methods of relative engine performance diagnostics', *SAE Transactions*: 2025-50.
- Ying, Yulong, and Jingchao Li. 2023. 'An improved performance diagnostic method for industrial gas turbines with consideration of intake and exhaust system', *Applied Thermal Engineering*, 222: 119907.
- Yoon, Jae Eun, Jong Jun Lee, Tong Seop Kim, and Jeong L Sohn. 2008. 'Analysis of performance deterioration of a micro gas turbine and the use of neural network for predicting deteriorated component characteristics', *Journal of Mechanical Science and Technology*, 22: 2516.
- Zwebek, A, and P Pilidis. 2003. 'Degradation Effects on Combined Cycle Power Plant Performance—Part II: Steam Turbine Cycle Component Degradation Effects', *J. Eng. Gas Turbines Power*, 125: 658-63.
- Zwebek, AI, and P Pilidis. 2004. 'Degradation effects on combined cycle power plant performance—Part III: Gas and steam turbine component degradation effects', *J. Eng. Gas Turbines Power*, 126: 306-15.